Electronic Supplementary Material (ESI) for Energy & Environmental Science.

+20°C **+40°C** **+50°C**

Figure S1. Pure fluoromethane (FM) phase change with increasing temperature. FM reaches superfluid state beyond critical point.

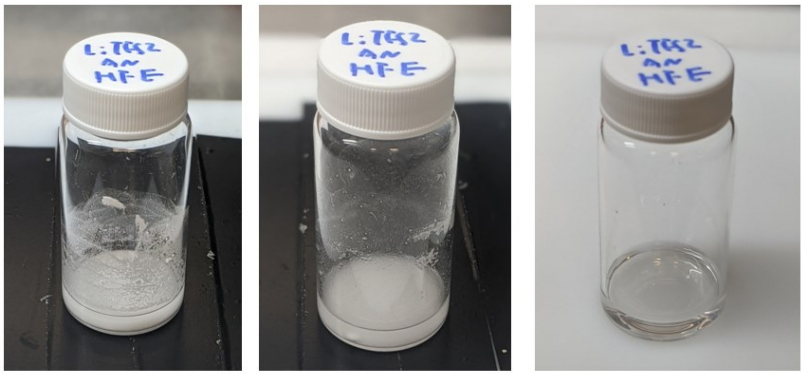

Figure S2. Solubility test of LiTFSI-AN-HFE mixture.

AN-based LHCE was made to compare with studied liquefied gas electrolyte. With the same amount of salt (1.2 M LiTFSI) in the studied liquefied gas electrolyte, 1 M AN in HFE dilute are not able to dissolve all the salt, indicating stronger Li^+ coordination from FM over HFE. The salt is properly dissolved in a mixture of 1.2 M LiTFSI, 3 M AN in HFE (AN to HFE around 1:6 in vol). However, even with three times of AN cosolvent, the conductivity of AN-based LHCE still much lower than the liquefied gas electrolyte in all the temperature range, which mainly results from HFE's higher viscosity and lower solvating ability over FM. In HFE dilute, a higher ratio of AN solvent may able to increase the conductivity but might also sacrifice Li metal stability due to the increased amount of free AN molecules.

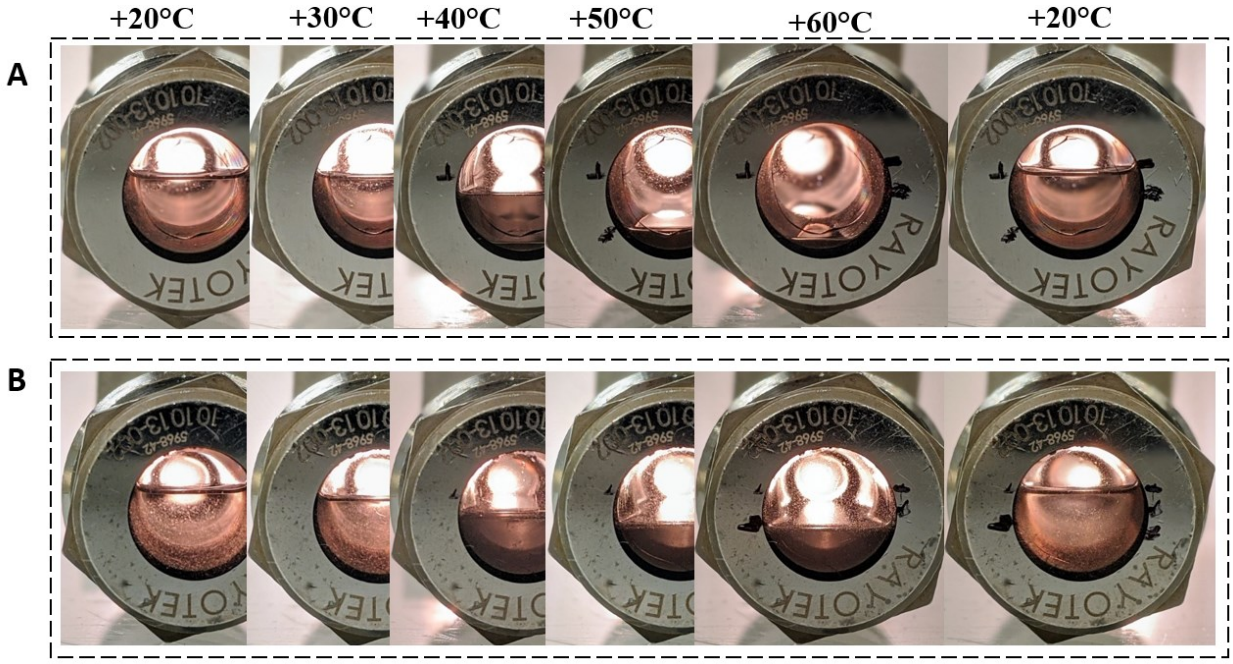

Figure S3. Phase changes of fluoromethane-based liquefied gas electrolytes with different amount of salt and cosolvent. (A) 0.1 M LiTFSI, 0.1 M AN in FM, (B) 1.2 M LiTFSI, 1 M AN in FM

Figure S4. Optical images of custom designed Raman cell

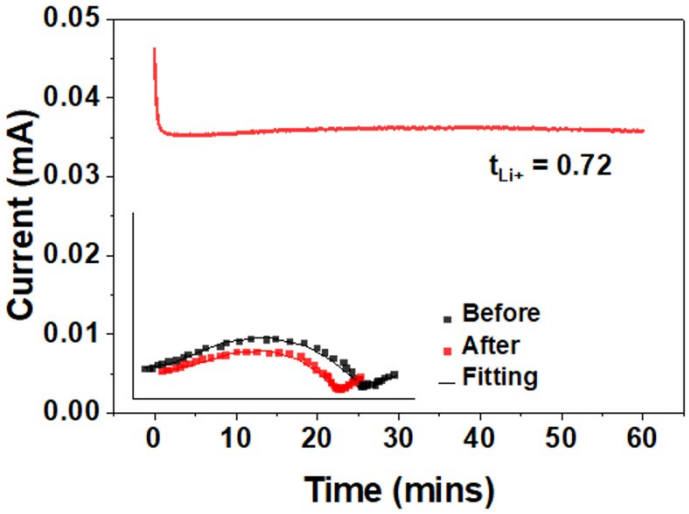

Figure S5. Polarization curve of 1.2 M LiTFSI-AN-FM electrolyte for Li^+ transference number. I_0 indicates the initial current, I_{ss} indicates the steady state current.

$$t_+ = \frac{I_{ss}\,(\Delta V - I_0 R_0)}{I_0(\Delta V - I_{SS} R_{SS})}$$

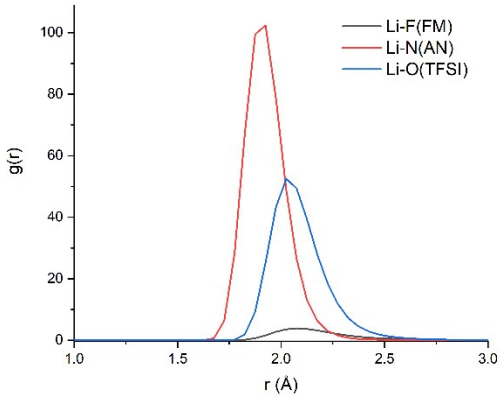

Figure S6. Radial distribution functions (RDFs) for the Li^+ cations with fluorine of FM, nitrogen of AN and oxygen of TFSI from MD simulations at for -20°C.

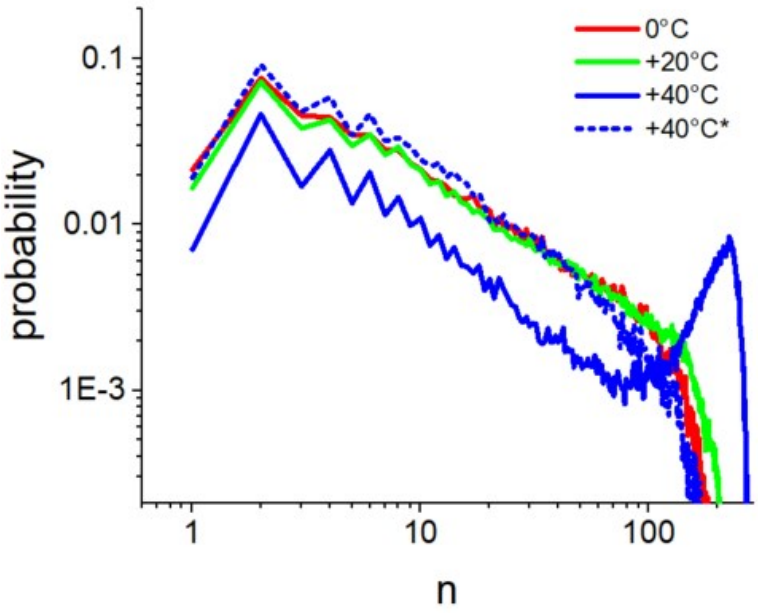

Figure S7. Probably of the Li^+ or $TFSI^-$ ions to participate in the ion aggregate of size (n) or free ions (n=1) from MD simulations. (40°C*) denotes a compressed electrolyte corresponding to density of regular electrolyte at 20°C.

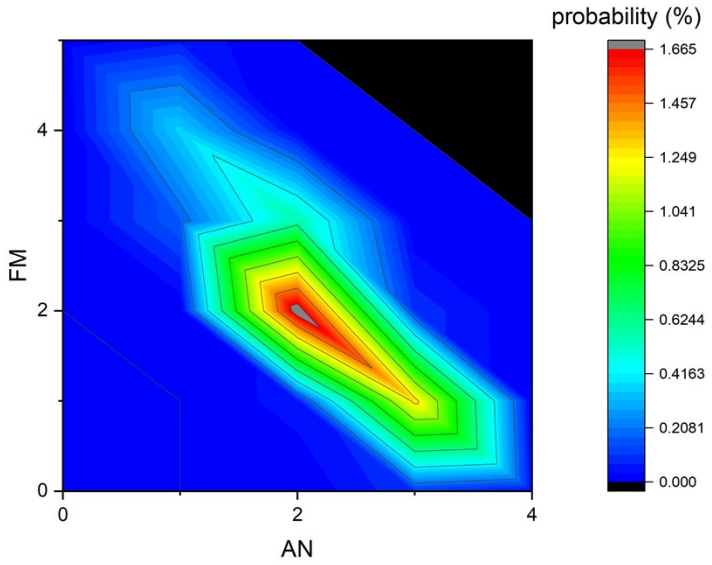

Figure S8. Probability of $Li^+(FM)_n(AN)_m$ solvation shells for the Li^+ cations not coordinated to any O(TFSI) within 2.8 Å from MD simulations at 253K. The most probably solvate is $Li^+(FM)_2(AN)_2$.

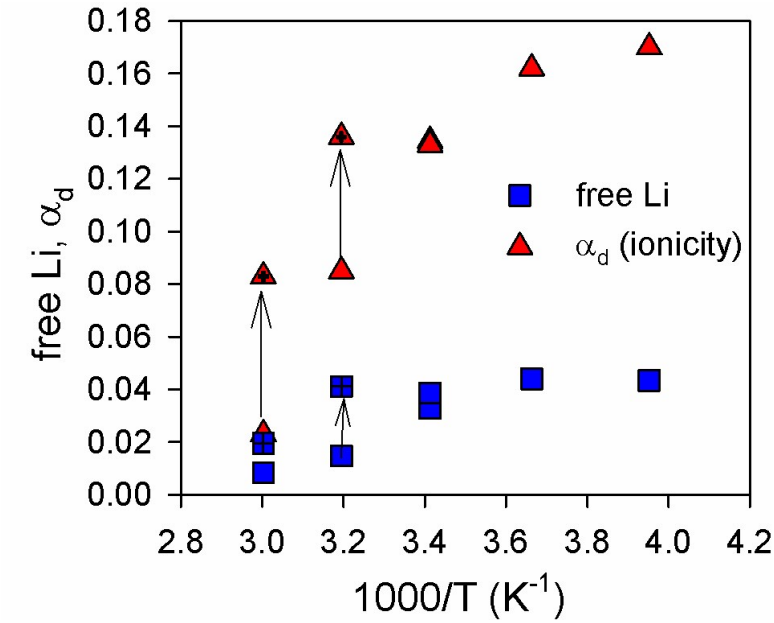

Figure S9. The fraction of free Li^+ cations and degree of dynamic dissociation α_d (ionicity). Crossed symbols denote a [more] compressed electrolytes. Arrows show changes of ionicity and fraction of free Li^+ as a result of electrolyte compression.

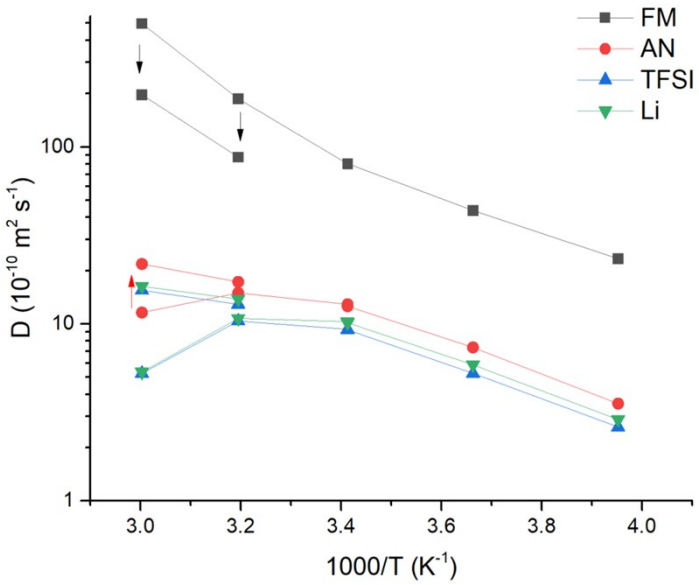

Figure S10. Self-diffusion coefficients from MD simulations. Arrows show changes of the self-diffusion coefficients as a result of electrolyte compression.

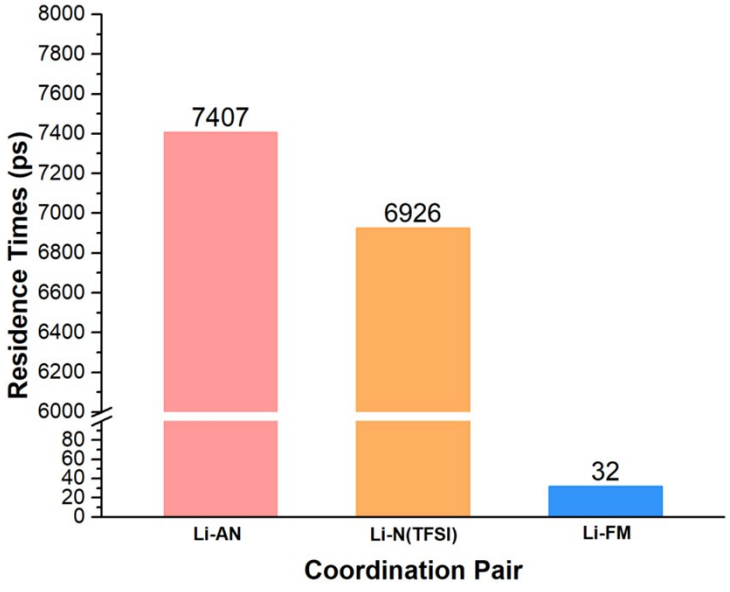

Figure S11. Residence time for different Li coordination at 0°C.

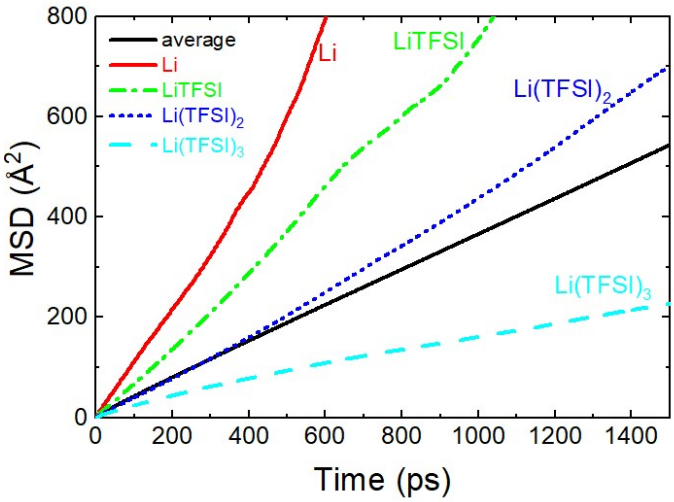

Figure S12. Mean-square displacement of free Li^+ with no N(TFSI) within 5.0 Å and Li^+ coordinated to 1,2,3 $TFSI^-$ anions using r(Li-N(TFSI)) < 5 Å criteria.

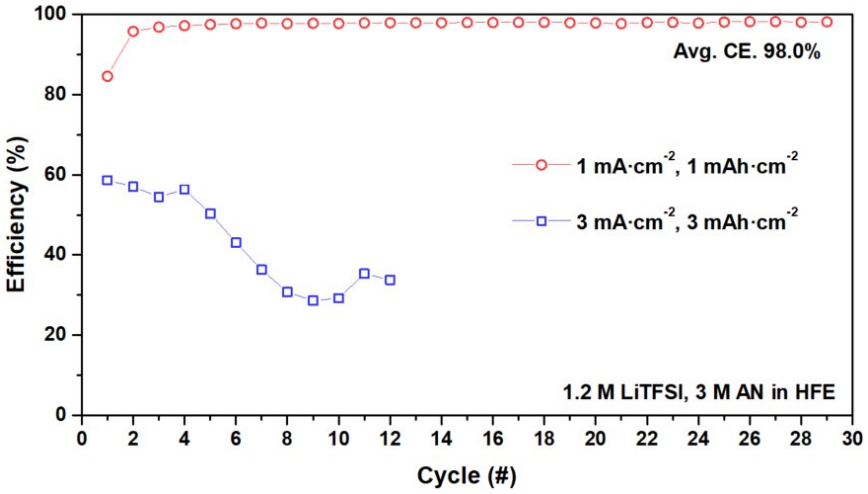

Figure S13. The CE of Li metal plating/stripping in 1.2 M LiTFSI, 3 M AN in HFE with different conditions.

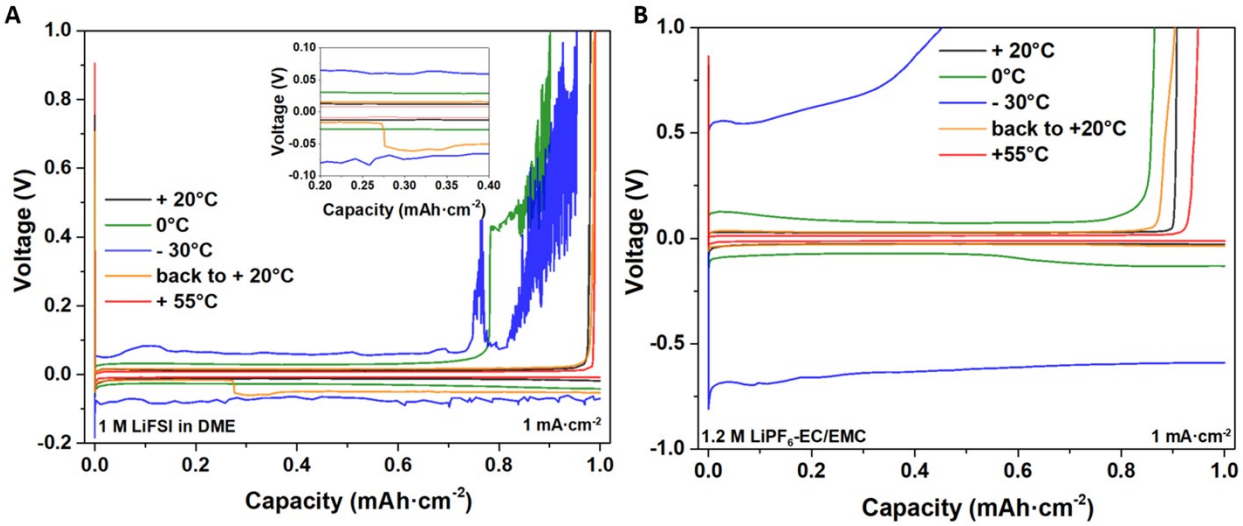

Figure S14. Voltage profiles for the Li metal half-cell using 1 M LiFSI in DME (**A**) and 1.2 M $LiPF_6$-EC/EMC (**B**) in Figure 2C.

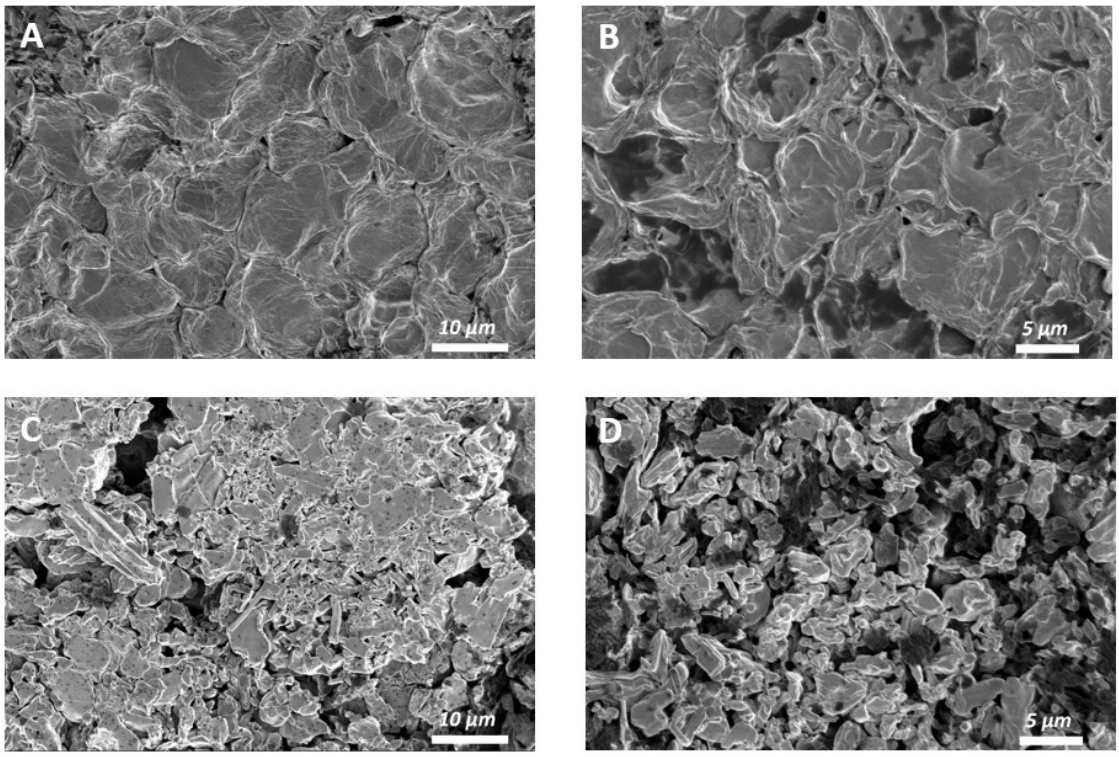

Figure S15. SEM characterizations of morphologies of cycled Li metal anode in Li/NMC cells in 1.2 M LiTFSI-AN-FM (**A-B**) and 1.2 M $LiPF_6$-EC/EMC (**C-D**) for 3 (**A, C**) and 50 (**B, D**) cycles. The cells were stopped and disassembled after discharge.

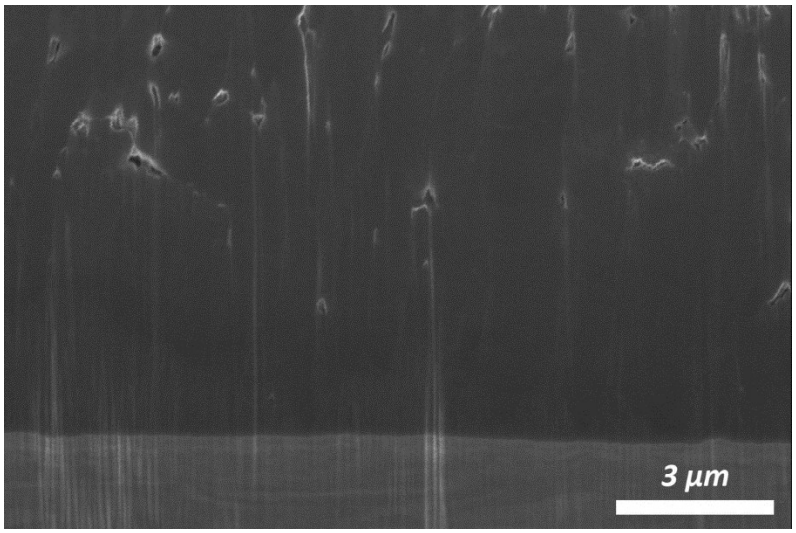

Figure S16. Cryo-FIB zoomed in image of Li/substrate interface. Li metal is deposited at -60°C in 1.2 M LiTFSI-AN-FM, at a current density of 0.5 $mA \cdot cm^{-2}$ with a capacity of 3 $mAh \cdot cm^{-2}$.

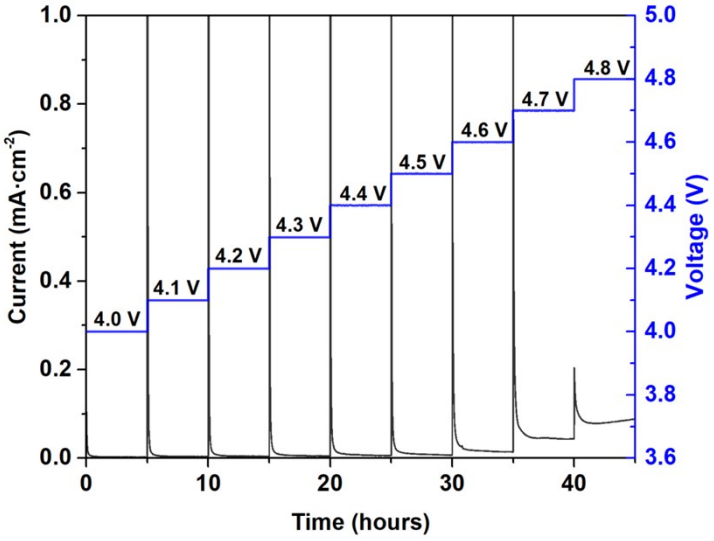

Figure S17. Li-NMC622 voltage hold test using 1.2M LiTFSI-AN-FM.

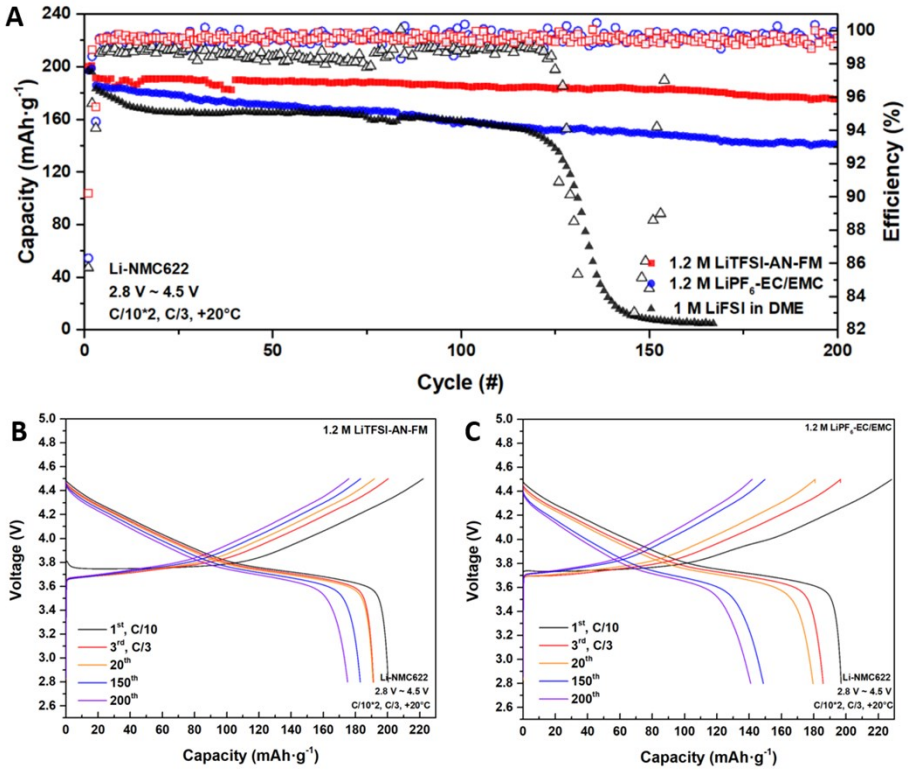

Figure S18. Cycling performance of Li-NMC622 cell at cut off voltage of 4.5 V using electrolyte of 1.2 M LiTFSI- AN-FM, 1.2 M $LiPF_6$-EC/EMC, and 1 M LiFSI in DME.

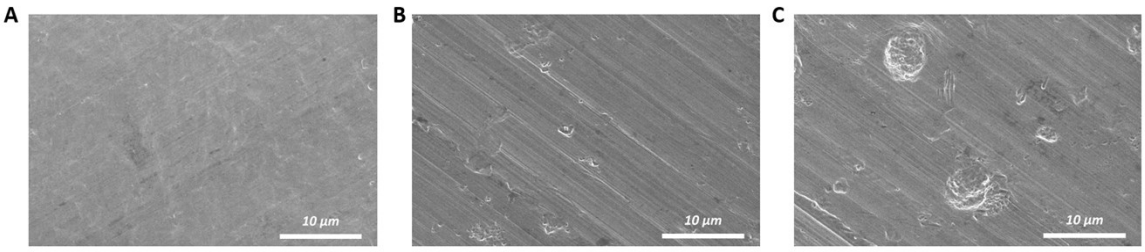

Figure S19. SEM images of Al current collectors of (A) fresh foil and (B, C) foil after 50 cycles with electrolytes (B) 1.2 M LiTFSI-AN-FM and (C) 1 M LiFSI in DME.

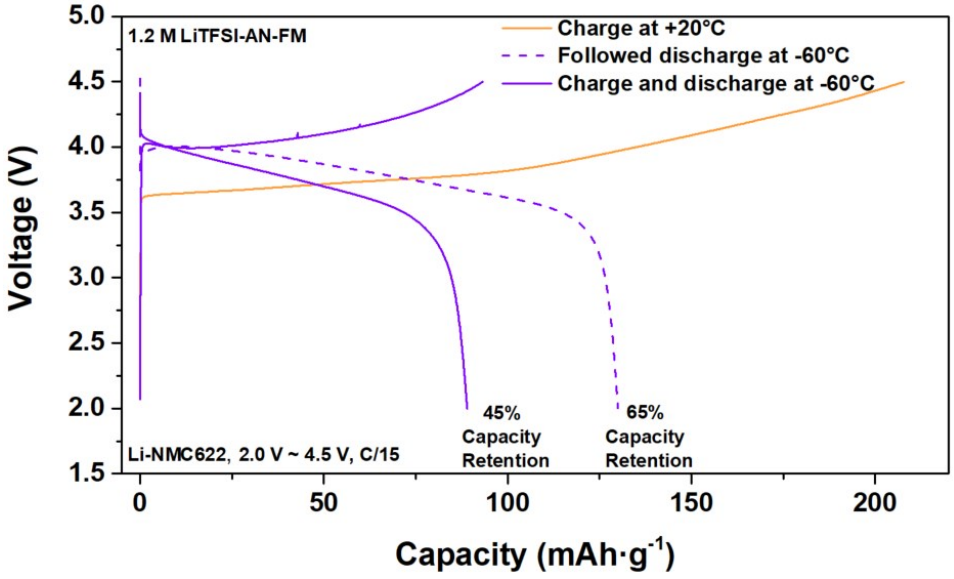

Figure S20. Low-temperature discharge curves. The cells were charged at different temperatures and discharged at -60°C using 1.2 M LiTFSI-AN-FM.

Figure S21. Li-NMC622 coin cell powers LED bulb at dry ice temperature (-78°C) using 1.2 M LiTFSI-AN-FM.

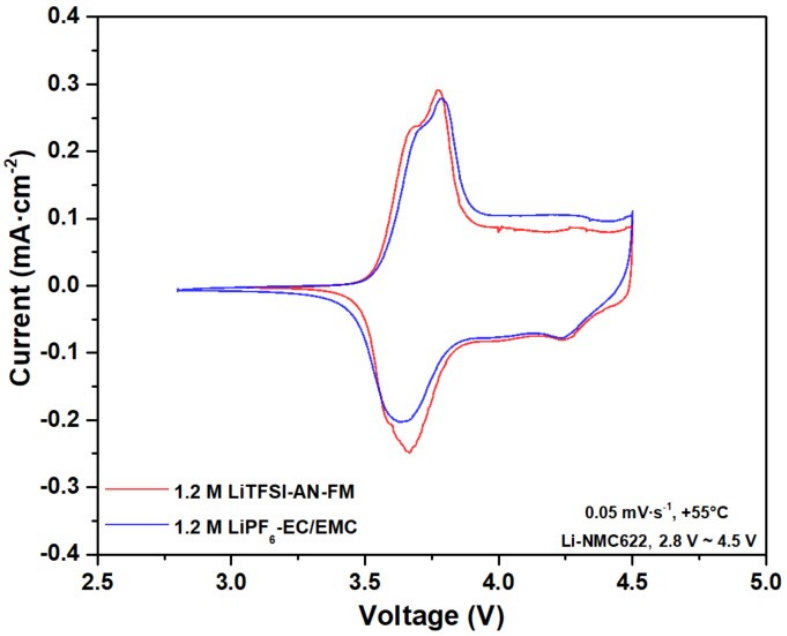

Figure S22. CV test of Li-NMC622 cell in voltage range of 2.8-4.5 V at +55°C in different electrolytes.

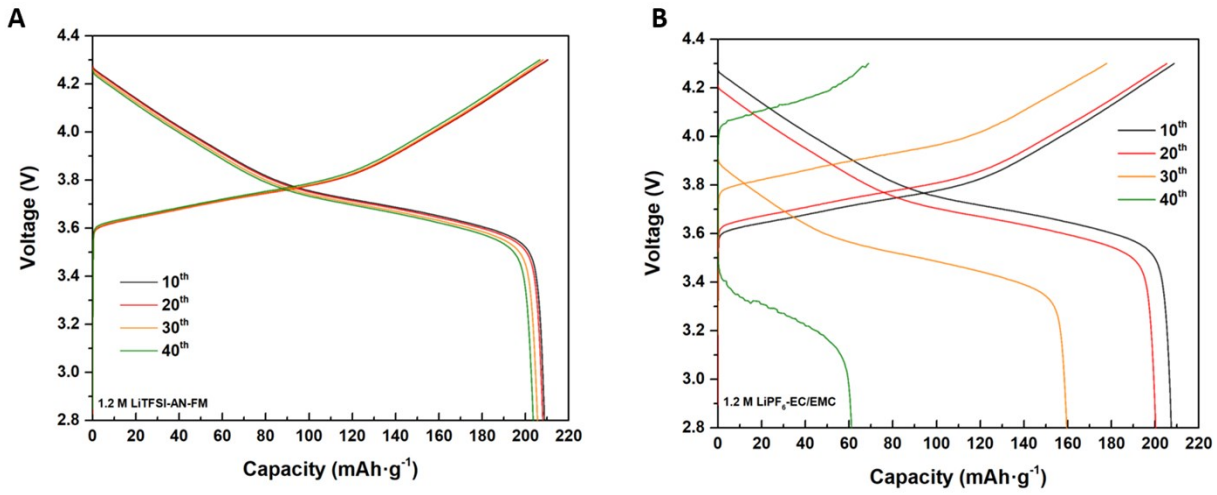

Figure S23. Voltage profiles of high temperature performance of Li-NMC622 cells in different electrolytes.

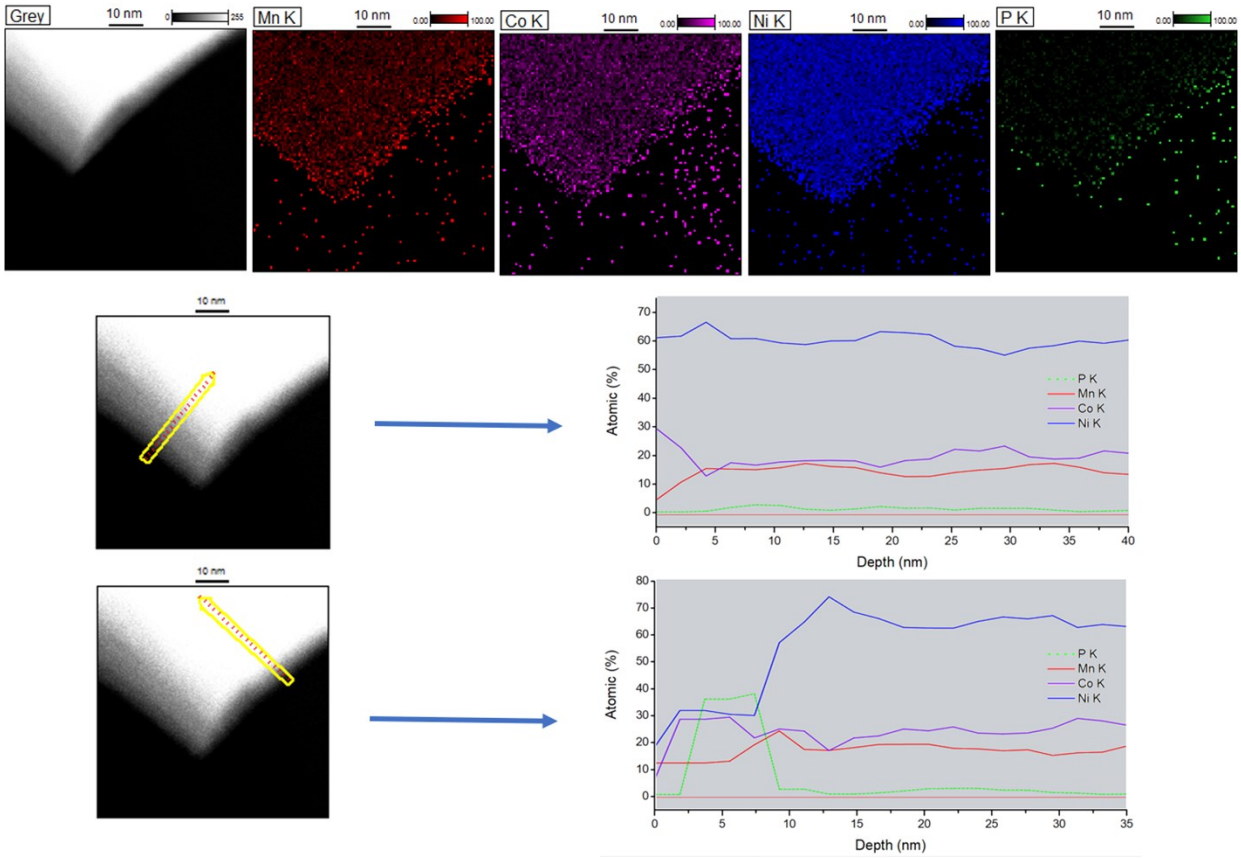

Figure S24. STEM-EDS spectra of CEI of the cycled NMC in 1.2 M $LiPF_6$-EC/EMC.

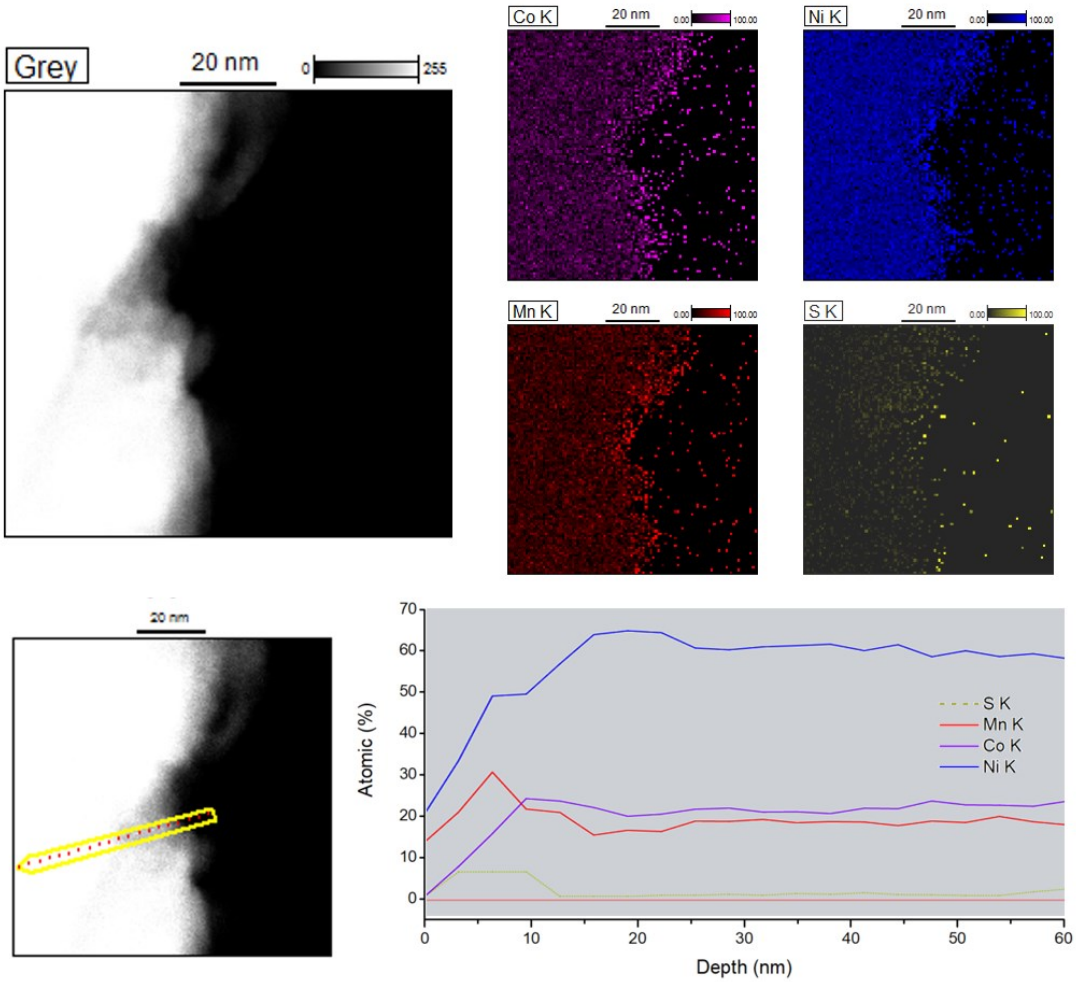

Figure S25. STEM-EDS spectra of CEI of the cycled NMC in 1.2 M LiTFSI-AN-FM

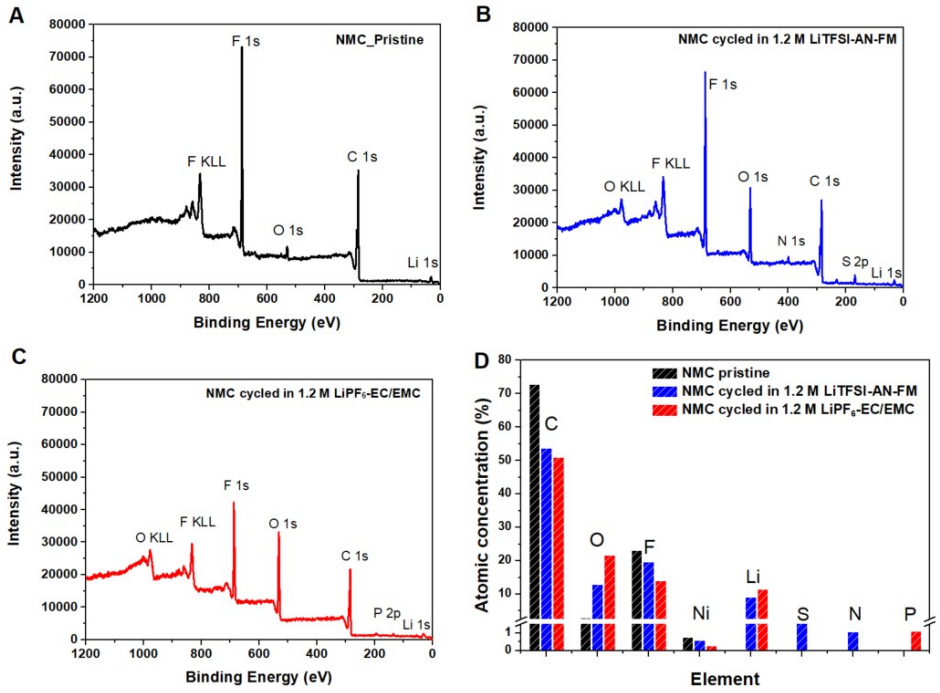

Figure S26. XPS spectra of the pristine NMC (**A**) and NMC electrodes cycled in 1.2 M LiTFSI-AN-FM (**B**), and 1.2 M $LiPF_6$ in EC/EMC 3:7 (**C**) and the atomic ratio summary (**D**). Li-NMC622 cell was cycled for 50 cycles (C/3, 2.8-4.3 V) and stopped in the discharge state.

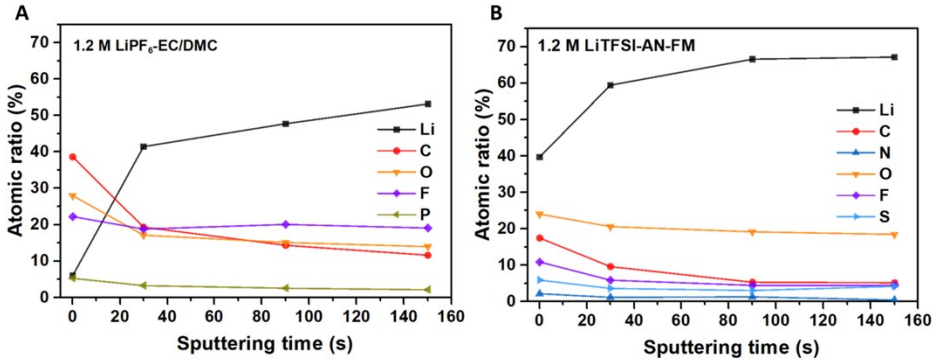

Figure S27. XPS quantified atomic composition ratios of Li-metal interface with various duration of Ar^+ sputtering cycled in 1.2 M $LiPF_6$-EC/EMC (**A**), and 1.2 M LiTFSI-AN-FM (**B**).

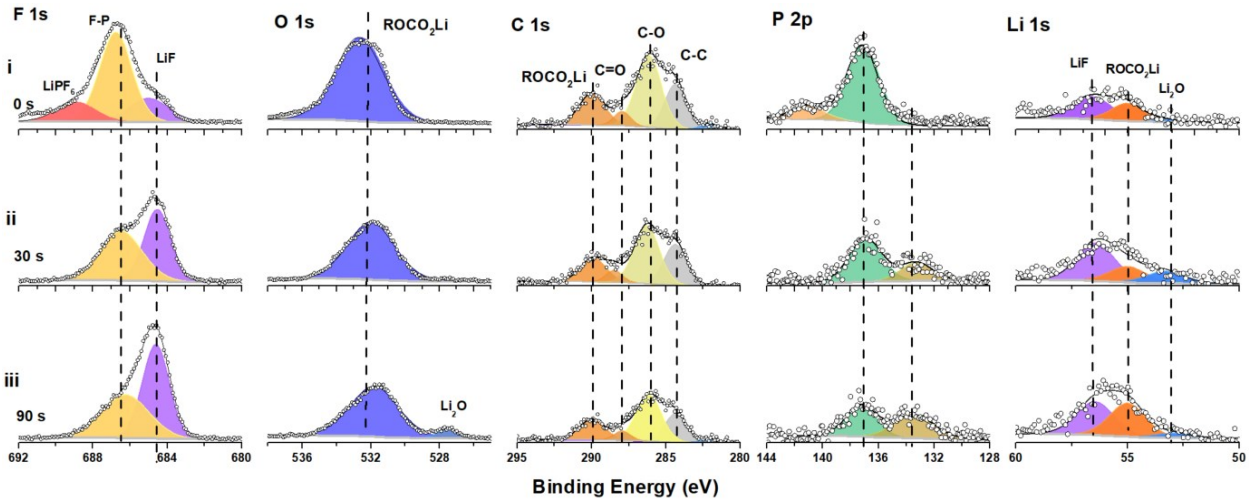

Figure S28. XPS analysis of SEI layers for the cycled Li metal in 1.2 M $LiPF_6$-EC/EMC. Li-NMC622 cell was cycled 50 cycles (C/3, 2.8-4.3 V) and stopped at discharge state.

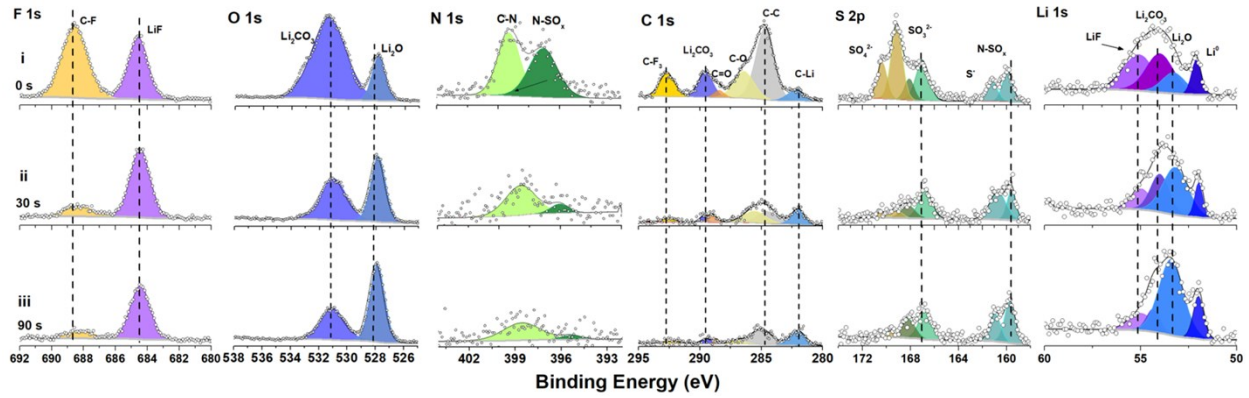

Figure S29. XPS analysis of SEI layers for the cycled Li metal in in 1.2 M LiTFSI-AN-FM. Li-NMC622 cell was cycled 50 cycles (C/3, 2.8-4.3 V) and stopped at discharge state.

The Ar^+ sputtering depth-profiling XPS was applied Li metal anodes after 50 cycles in Li-NMC cells in different electrolytes (**Figure S27-29**). Before Ar^+ sputtering, the SEI formed in the carbonate-based electrolyte has a low Li ratio (< 10%) and a high carbon ratio (> 40%) (**Figure S27A**), indicating that the SEI is mainly composed by organic-like species, such as Li alkyl carbonates ($ROCO_2Li$) (**Figure S28**). Conversely, as shown in **Figure S27B**, the SEI in liquefied gas electrolyte shows the opposite trend (Li ~ 40%, C < 20%), where the SEI is dominated by inorganic species, including Li_2CO_3, LiF, and Li_2O (**Figure S29**). The FSI^- decomposition is confirmed by S 2p and N 1s spectra. The chemistry of the internal SEI layer is revealed by steps of Ar^+ sputtering. As expected, there is an increase of Li signal and a decrease of other elements for both electrolytes, including C, O, and F. This suggests there is an increasing amount of inorganic species in the inner layer. However, the SEI formed in liquefied gas electrolyte still has a higher Li ratio and a lower C ratio in comparison to the carbonate-based electrolyte after each sputtering step (**Figure S27B, S29**). Although the SEI in carbonate electrolyte has more LiF formed by the decomposition of $LiPF_6$, the large amount of Li alkyl carbonates and heterogeneous distribution of LiF results in a SEI with poor ionic conductivity and low stability towards the electrolyte.[1,2] In contrast, the inorganic-rich SEI formed by the decomposition of FM, CO_2, and $TFSI^-$ in liquefied gas electrolyte enables a robust interface for aggressive Li metal cycling.[3]

Table S1. Properties of the FM-AN-LiTFSI electrolytes from MD simulations and simulation parameters.

T (°C)	-20	0	20	20	40	60	40*	60*
# c (M)	1.47	1.35	1.20	1.20	0.93	0.54	1.20	0.93
Equilibration run(ns)	100	100	100	40	100	27	20	49
Production run (ns)	166	133.748	164.81	40	108	55.3	45	48.5
Box size (Å)	54.64	56.15	58.38	58.38	63.63	76.03	58.38	63.63
Density (kg m^{-3})	1164	1072	954	954	737	432	954	737
conductivity (mS cm^{-1})	6.1	10.0	12.0	12.0	6.0	0.4	15.6	8.2
viscosity (mPa *s)	1.14	0.515	0.28	0.283			0.245	0.21
α (eq. 1)	0.49	0.50	0.51	0.50			0.5	0.49
β (eq. 1)	0.97	0.91	0.93	0.94			0.92	0.98
$\mathbf{t}_+$ (eq. 3)	0.96	0.96	0.98	0.96			0.96	0.94

Reference

1. Aurbach, D. The Surface Chemistry of Lithium Electrodes in Alkyl Carbonate Solutions. *J. Electrochem. Soc.* **141**, L1 (1994).

2. Aurbach, D. Review of selected electrode-solution interactions which determine the performance of Li and Li ion batteries. *J. Power Sources* **89**, 206–218 (2000).

3. Zhang, Q. *et al.* Synergetic Effects of Inorganic Components in Solid Electrolyte Interphase on High Cycle Efficiency of Lithium Ion Batteries. *Nano Lett.* **16**, 2011–2016 (2016).